Rheology of Confined Polymer Melts

Rajesh Khare,[†,‡] Juan J. de Pablo,[†] and Arun Yethiraj*[,‡]

Department of Chemical Engineering, and Theoretical Chemistry Institute and Department of Chemistry, University of Wisconsin, Madison, Wisconsin 53706

Received January 22, 1996; Revised Manuscript Received August 12, 1996[⊗]

ABSTRACT: The behavior of confined polymer melts in a shear flow is investigated using molecular dynamics simulations. Polymer molecules are modeled as bead−spring chains that interact via repulsive site−site potentials. The fluid is contained between atomistic walls and shear is imparted by moving the walls in opposite directions to simulate planar Couette flow. Experimental conditions are simulated by maintaining the walls at a constant temperature. The density, velocity, and temperature profiles during shear flow are monitored and compared to those of simple liquids under similar conditions. For the shear rates investigated, polymeric fluids exhibit a much stronger tendency for slip at the wall−fluid interface than simple fluids. The magnitude of slip increases with increasing shear rate. For short chains the magnitude of slip increases with increasing chain length but appears to reach an asymptotic value at approximately the entanglement length. The viscosity increases as the film thickness is decreased, in qualitative agreement with surface forces apparatus experiments. The chains stretch and align in the flow direction when sheared.

1. Introduction

The behavior of confined polymer melts in shear flow is of importance in several practical applications such as lubrication and polymer processing. For example, an important consideration in polymer extrusion operations is the surface finish of the extrudate, which is governed largely by the flow behavior at the polymer−wall interface.[1] There is therefore considerable interest in establishing a cause−effect relationship between polymer−surface interactions and melt flow behavior.

In engineering applications, flow processes are usually modeled using macroscopic equations, the solution of which requires specification of appropriate boundary conditions and numerical values of transport coefficients (e.g. viscosity and thermal conductivity). The most commonly employed boundary condition is that of no-slip (or stick) at the wall, which assumes that the wall and fluid layer next to it move with the same velocity. Continuum mechanics analyses often assume that the transport coefficients of the confined fluid are the same as those of a bulk fluid. Recent experiments have called both of these assumptions into question (see below). The long-term goal of this research is to employ molecular simulation to bridge the gap between the "microscopic" and "macroscopic" pictures of flow behavior, thereby providing some insight into atomistic scale hydrodynamics near the surface as well as the effect of confinement on transport properties. In this paper we focus on a simple model of polymer molecules, i.e. bead−spring chains that interact via purely repulsive potentials, and study the effect of shear flow and confinement on the conformational, structural, and dynamic properties of the fluid.

Experiments have suggested that slip may occur at polymer−wall interfaces for high enough values of shear rate, particularly when polymer−surface interactions are weak. Rheometric and extrusion experiments on polyethylene[1,2] have shown that the onset of surface melt fracture (sharkskin) coincides with a discontinuity in the slope of a shear stress vs shear rate plot. These observations were attributed to the occurrence of slip at the polymer−wall interface. More direct evidence of slip at the surface was provided by Migler et al.,[3] who measured the velocity of a sheared polymer melt at the polymer−wall interface using a combination of evanescent-wave-induced fluorescence (EWIF) and fringe pattern fluorescence recovery after photobleaching (FPFRAP).

The transport coefficients used in continuum analyses of the flow behavior of confined polymers also need careful consideration. Their values are usually extracted from experimental data for macroscopic systems. However, surface forces apparatus experiments have clearly shown that the flow properties of molecularly thin liquid films are substantially different from those of bulk liquids[4−10] for systems as diverse as cyclohexane and octamethylcyclotetrasiloxane (these molecules may be considered quasi-spherical),[4−7,9] linear alkanes,[4,6,7,9] branched alkanes,[6] and polymer melts.[8] These studies found that, in general, the viscosity of thin films was similar to that of the bulk fluid for films thicker than about 8−10 molecular diameters. If the film thickness was decreased to about 6 molecular diameters, the viscosity of the thin films could become as large as 5 orders of magnitude higher than the bulk value, and the molecular relaxation times could become 10 orders of magnitude larger than those in the bulk. Films that were only 3−4 molecular diameters thick started to exhibit solidlike behavior, including the appearance of a yield stress.

In light of these experimental findings, it would be helpful to have a theoretical method for direct determination of transport coefficients and boundary conditions. We have therefore undertaken simulation studies which combine molecular and macroscopic approaches while directly simulating the flow conditions. Such simulations have the attractive feature of yielding direct information about the various molecular level processes occurring in the flow of confined fluids while also providing estimates for the transport coefficients.

A number of molecular simulations of shear flow have appeared in the literature.[11−19] These can be broadly classified into homogeneous shear methods and surface-driven shear methods. In homogeneous shear methods,[11] the shear flow is simulated by modifying the

[†] Department of Chemical Engineering.
[‡] Theoretical Chemistry Institute and Department of Chemistry.
[⊗] Abstract published in *Advance ACS Abstracts,* October 15, 1996.

S0024-9297(96)00083-6 CCC: $12.00

equations of motion of the molecules and using sliding wall periodic boundary conditions. This technique is meant to describe a small region of a bulk fluid under shear; the confining boundary is not modeled explicitly. In surface-driven shear methods, shear is imparted on the fluid through the actual motion of the confining walls. Since the confining surface is modeled explicitly, a systematic investigation of the boundary condition as a function of solid and fluid properties is possible, thereby making the latter approach more suitable for our work.

Surface-driven shear simulations have been used to study the behavior of simple liquids and short chains in shear flow.[12−19] These studies have employed various types of walls: fluidlike,[12,14,15] stochastic, structureless,[13] and those comprised of atoms rigidly attached by stiff springs to crystalline lattice sites.[16] Different types of solid walls did not seem to qualitatively alter the flow behavior. Thompson et al.[16−18] found that for small film thicknesses of about 3 molecular diameters, spherical molecules crystallize while short chain molecules enter a glassy state. Chain molecules were seen to exhibit shear thinning behavior at simulated shear rates. Manias et al.[19] simulated Couette flow of hexamers in channels of thickness 4−6 atomic diameters. By varying the strength of the wall−fluid interaction, they observed a wide range of boundary conditions: no-slip, slip at the wall−fluid interface, and even slip within the fluid. A strong correlation between velocity and density profiles was observed, and slip was found to occur in low density areas where interfaces (between the fluid and a solid wall or between an absorbed layer and the bulk fluid) were present.

There are several reasons why we believe that previous work does not properly address the behavior of confined polymer melts under shear. First of all, most previous simulations (surface-driven shear[18,19] as well as homogeneous shear[11]) imposed a constant temperature across the entire fluid film using a variety of thermostating mechanisms. At high shear rates, this is unrealistic because the viscous heat generated in the fluid is artificially and instantaneously removed, which can only happen in a fluid with infinite thermal conductivity. Our simulations mimic more closely the experimental setup because the only temperature control is provided by a coupling between the walls and a heat bath. Second, we investigate films thicker than those previously considered, thereby permitting the development of both a well defined solid−fluid interface and a bulklike homogeneous fluid far from the walls. Third, we study longer chains (lengths up to $N = 165$). This is important, since the entanglement length in bead−spring chains is believed to be about $N = 50$.

The main conclusions of this work are as follows. Polymeric fluids exhibit a much stronger tendency for slip at the wall−fluid interface than simple fluids. The magnitude of slip increases with increasing shear rate. The amount of slip increases with molecular weight for short chains and appears to reach an approximately constant value for chain lengths on the order of the entanglement length. Confinement increases the magnitude of slip and the viscosity. The chains stretch and align in the flow direction under shear.

The rest of the paper is organized as follows: In section 2 we describe our simulation approach; in section 3 we present results for the flow properties, effect of confinement, chain conformations, and slip behavior; and in section 4 we present our conclusions.

2. Simulation Method

The simulated system consists of the sheared fluid confined between two atomistic walls. The atoms that comprise the walls and the beads on the polymer chains interact via a continuous repulsive Lennard−Jones site site potential, $\phi^{LJ}(r)$, given by

$$\phi^{LJ}(r) = 4\epsilon\left[\left(\frac{\sigma}{r}\right)^{12} - \left(\frac{\sigma}{r}\right)^{6} + \frac{1}{4}\right]\theta(r_c - r) \qquad (1)$$

where $\theta(r)$ is the Heaviside step function, σ and ϵ are the Lennard−Jones parameters, and $r_c = 2^{1/6}\sigma$. This potential corresponds to the usual Lennard−Jones potential that is truncated at the minimum and shifted; it is often referred to as the Weeks−Chandler−Andersen (WCA) potential. In the rest of the paper we use σ, ϵ, and $\tau = (m\sigma^2/\epsilon)^{1/2}$ to set length, energy, and time scales, respectively (m is the mass of an atom). Temperature is reported in reduced units of ϵ/k, where k is Boltzmann's constant, and all other quantities are reported in reduced units obtained by appropriate combinations of σ, ϵ, τ, and ϵ/k.

The actual value of the shear rate (in inverse seconds) depends on how our model is mapped onto a real fluid. If each bead is considered to represent a CH_2 group on polyethylene, and we use Lennard−Jones parameters of $\sigma = 3.93$ Å and $\epsilon/k = 47$ K, a reduced shear rate of $\gamma = 0.1$ corresponds to an actual shear rate of 4.3×10^{10} s^{-1}. Often each bead in a coarse-grained model is meant to represent a collection of two or three CH_2 groups. In this case the actual shear rate would be considerably lower than 10^{10} s^{-1}, depending on the values employed for the Lennard−Jones parameters.

The walls consist of a single layer of atoms attached to face-centered cubic (FCC) lattice sites by stiff harmonic springs. A high value of the force constant of these springs is used in this work to ensure that the mean square displacement of wall atoms is below the Lindemann criterion for melting.[16,20] The FCC lattice has an edge length of 1.3, so that the nearest neighbor distance between wall atoms is 0.92; such a value ensures that fluid atoms do not leak through the walls during simulation.

The polymer chains are modeled as bead−spring chains. The beads interact with each other and with the wall atoms via the repulsive Lennard−Jones potential (eq 1). The springs are represented by a finitely extendable nonlinear elastic (FENE) potential:

$$\phi^{FENE}(r) = -\frac{\kappa Q^2}{2}\ln\left[1 - \left(\frac{r}{Q}\right)^2\right] \qquad (2)$$

where κ is the spring constant and Q is the maximum extension of the spring. We use values of $\kappa = 100$ and $Q = 1.5$; these values ensure that unphysical chain crossings are prevented.[21] The resulting bond length is approximately 0.9σ.

In our coordinate system the walls are parallel to the xy plane and are separated by a distance H in the z direction. Periodic boundary conditions are used in the x and y directions. Shear is imposed on the system by moving the lattice sites to which the wall atoms are attached at a constant velocity. The two walls are moved with the same velocity but in opposite directions along the x axis. The trajectories of fluid atoms are determined using a simple velocity Verlet algorithm. The wall temperature is kept constant by coupling the motion of the wall atoms to a heat bath maintained at the desired temperature.[17] The trajectories of the wall atoms are calculated by a stochastic generalization of the velocity Verlet algorithm.[22] Unless indicated otherwise, all the results reported here correspond to the following simulation conditions: $T_{wall} = 4.0$, $\rho = 0.8$, and chain length N = 20. Simulations are carried out using a time step of 0.002τ.

Initial configurations for chain lengths $N \leq 50$ are generated using a growth and equilibration algorithm.[23] For $N \geq 100$, initial configurations are first generated using the same algorithm but for a bead diameter of 0.75σ. The bead diameters are then increased to the desired value in three stages of short molecular dynamics simulations. This proce-

dure appears to produce well-equilibrated initial configurations. All simulations consist of an equilibration stage of 300 000 steps followed by a production run of at least 700 000 time steps. All properties of the system are confirmed to be time independent and symmetric about the central plane of the fluid film. Longer runs are carried out for simulations at the lowest shear rates studied here. All the profiles reported here are obtained by block averaging over blocks of 50 000 time steps each. Within each block, averages are determined by sampling every 20th time step. The quantities in the z direction are calculated by averaging over bins of size $= 0.5\sigma$.

The molecular model places constraints on the size of the simulation cell because there have to be an integral number of rows of wall atoms in the x and y directions and an integral number of chains. The simulations for $N = 20$ employ 93 chains in a box having dimensions $11.7 \times 11.7 \times 18.0$. Larger systems are used for simulations of longer chains. The largest system simulated consists of 87 chains of length $N = 165$ in a box of dimensions $32.5 \times 32.5 \times 18.0$. For comparison, simulations are also carried out for simple fluids. These simulations employ 1471 particles in a box of dimensions $10.4 \times 10.4 \times 18.0$. Except when investigating the effect of confinement, the separation between the walls is fixed at $H = 18\sigma$ in all simulations. In confined systems, the definition of the average fluid density can be ambiguous. In this work, we calculate the average density by assuming that the fluid cannot occupy a volume of thickness 0.5σ at either wall since the walls atoms effectively exclude the fluid from this region.

3. Results and Discussion

3.1. Density Profile and Flow Properties of Polymer Melts near Solid Surfaces. An important structural characteristic of confined fluids is a wall-induced layering in the direction normal to the walls. We begin our analysis by comparing the site density profiles under shear of simple, monomeric fluids to those of polymer melts. Figure 1a depicts the site density profile for a monomeric fluid at a nominal shear rate $\dot{\gamma} = 0.2$ and wall temperature $T_{\text{wall}} = 4.0$. Figure 1b shows the site density profile for a 20-mer chain fluid at the same nominal shear rate and $T_{\text{wall}} = 4.0$. In both figures, wall atoms are attached to lattice sites at $z = 0$ and 18 and the density profiles are normalized by the average density between $z = 0$ and 18. In both cases, the fluid is seen to be divided into two distinct regions: a wall−fluid interfacial region, where the walls induce significant ordering, and a bulklike, homogeneous fluid region in the central part of the film. At least three well-defined fluid layers next to the walls are observed for simple fluids, while only one well-defined layer is found in the polymeric fluid. Also, the height of the first peak near the wall is much smaller for the polymer melt than for the simple fluid. Similar results have been reported at equilibrium.[23,24] The differences in density profiles between simple liquids and polymers arise because chains do not pack against the wall quite as efficiently as simple liquids, and polymer molecules suffer a loss in configurational entropy near the surface.

The density profiles are insensitive to chain length for $N \leq 50$. As the chain length is increased further, some differences appear and are quite pronounced for $N = 165$. Figure 1c compares the density profiles for $N = 20$ and 165. For $N = 20$ there is a weak tendency to form three layers next to the wall, but for $N = 165$ there are only two layers. As a result, the height of the first peak in the density profile is higher for $N = 165$ chains than it is for $N = 20$. This behavior could be a manifestation of confinement since the film is effectively thinner (relative to the size of molecules) for the longer chains.

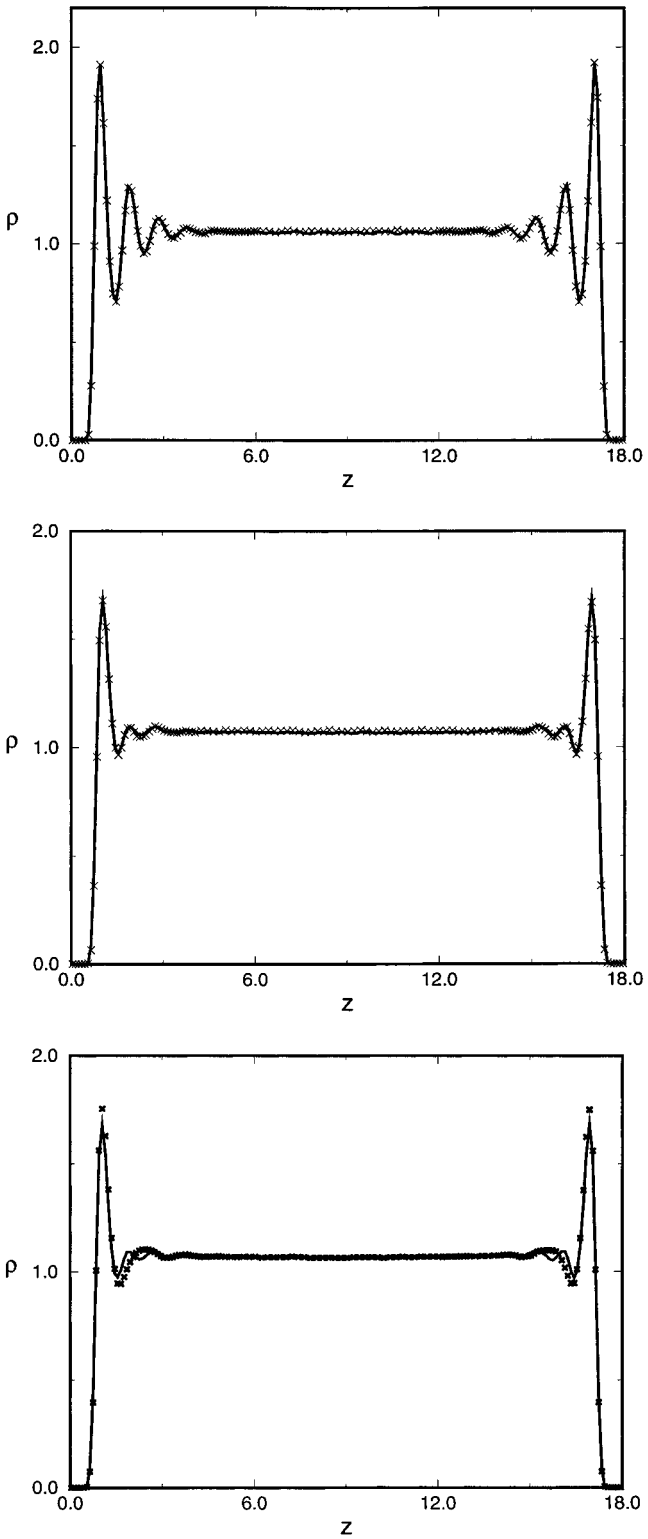

Figure 1. Density profiles for $H = 18$ and (a) $N = 1$, $T_{\text{wall}} = 4.0$, $\rho = 0.8$, $\dot{\gamma} = 0.2$ (line) and 0 (crosses); (b) $N = 20$, $T_{\text{wall}} = 4.0$, $\rho = 0.8$, $\dot{\gamma} = 0.2$ (line) and 0 (crosses); and (c) $T_{\text{wall}} = 4.0$, $\rho = 0.8$, $N = 20$ (line) and $N = 165$ (crosses).

Figure 1, parts a and b, also shows that for both simple liquids and polymers the density profiles under shear ($\dot{\gamma} = 0.2$) and at equilibrium are identical within the statistical uncertainty of the data. We find that the density profiles are relatively insensitive to shear rate even for the highest shear rates we have investigated. This is somewhat surprising, because the tendency of polymer molecules to orient preferentially along the surface[25] is enhanced by the presence of flow. Appar-

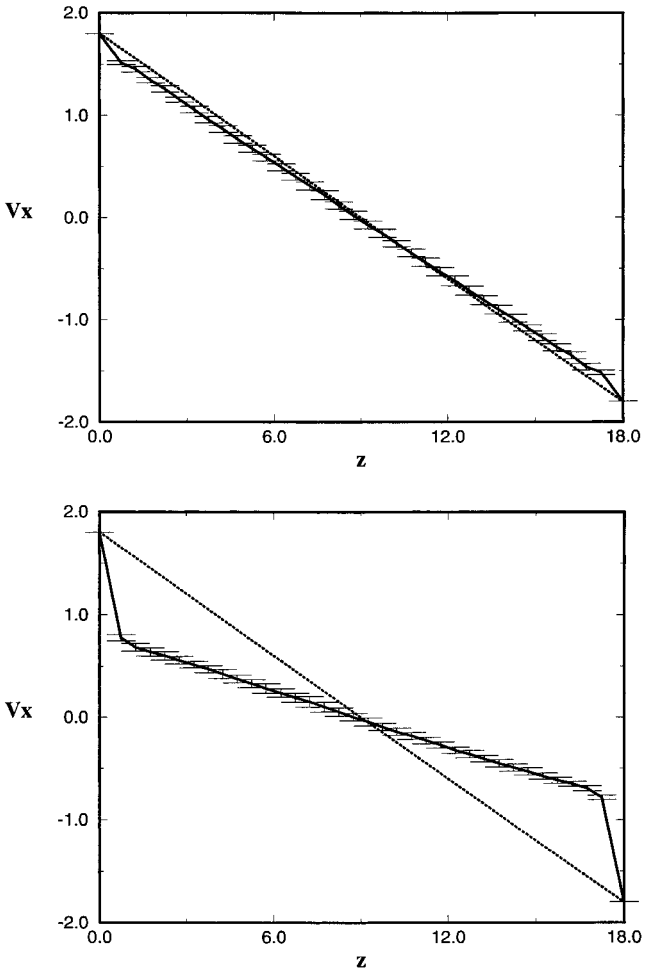

Figure 2. Velocity profiles for H = 18 and $\dot{\gamma} = 0.2$ for (a) $N = 1$, $T_{wall} = 4.0$, $\rho = 0.8$ and (b) $N = 20$, $T_{wall} = 4.0$, $\rho = 0.8$. The profile shown by dotted lines is the continuum mechanics prediction with no-slip boundary conditions.

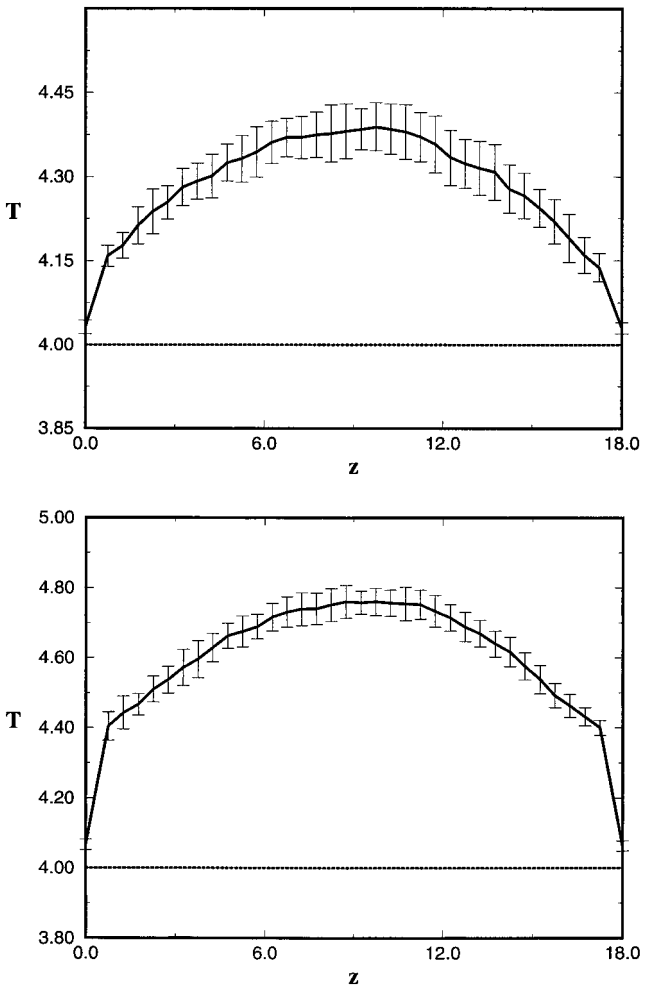

Figure 3. Temperature profiles for H = 18 and $\dot{\gamma} = 0.2$ for (a) $N = 1$, $T_{wall} = 4.0$, $\rho = 0.8$ and (b) $N = 20$, $T_{wall} = 4.0$, $\rho = 0.8$. The dotted line shows the wall temperature.

ently this increased orientation does not affect density profiles.

For no-slip boundary conditions and Couette flow, continuum mechanics predicts a linear velocity profile between the surfaces. Parts a and b of Figure 2 compare the velocity profiles obtained by simulation to those predicted by continuum mechanics. Simple fluids (Figure 2a) show a small tendency for slip at the walls, which is indicated by a small discontinuity of the velocity profile. Except for a region of thickness σ near the wall, the velocity profile is linear over the entire channel, and the actual shear rate (slope of the profile) is nearly identical to the nominal (imposed) shear rate. For the polymeric fluid (Figure 2b), although the velocity profile is once again linear over the entire channel (except for a region of thickness σ near the walls), large slip is observed near the walls. Slip has also been observed previously in simulations of short chains.[18,19] As a result of this large slip, the actual shear rate is much smaller than the nominal shear rate. Note that all the interactions (most importantly the wall−fluid interactions) are the same in both cases, and the different slip behavior observed is purely a consequence of the connectivity of the polymeric fluid. The velocity profiles are qualitatively similar for different chain lengths. Quantitative differences in these, which are manifest in the slip behavior, are discussed in more detail in a later section.

The temperature profiles for simple fluids are also different from those for polymers. Figure 3a shows that the temperature profile in a simple fluid under shear is roughly parabolic, as expected from continuum mechanics. A small temperature drop (discontinuity) is observed at the walls, which is consistent with the velocity slip reported above. Such a drop is more pronounced for polymeric fluids (Figure 3b). A parabolic temperature profile is also obtained for the polymeric fluid, but the temperature rise is higher for polymers than it is for simple fluids (at the same nominal shear rate). We find that temperature profiles are insensitive to chain length for chains of up to 165 segments.

The rheological behavior of polymer melts under shear is generally characterized in terms of their viscosity. In this work, the viscosity of the sheared fluid is determined as the ratio of the shear stress in the film (which we measure at the wall) to the shear rate. As stated above, because of the slip at the walls, the actual shear rate in the fluid is significantly different from the nominal shear rate, and different results are obtained depending on which shear rate is used to calculate viscosity. We refer to these two viscosities as the nominal and the actual viscosities. Figure 4 depicts these viscosities as a function of the corresponding shear rate. Not only are actual and nominal viscosities different, but the shear rate dependence is also different. The actual viscosity curve indicates that the polymeric fluid shows shear thinning behavior up to an actual shear rate of 0.2, beyond which the viscosity hardly changes with shear rate. We compare these results with those obtained by Xu et al.[21] for $N = 20$ chains under

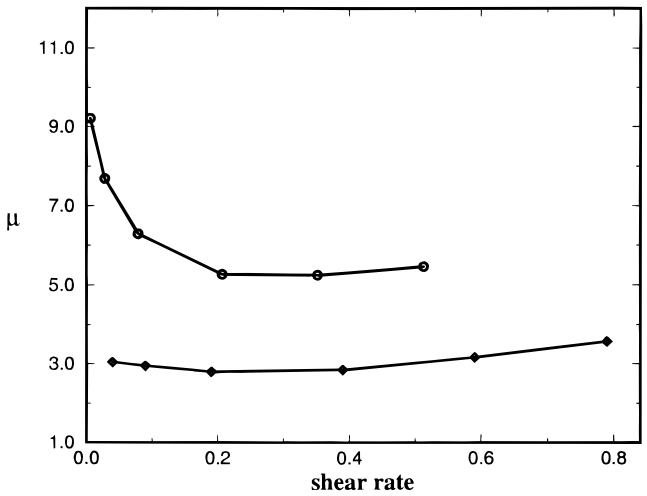

Figure 4. Viscosity as a function of shear rate for $N = 20$, $H = 18$, $T_{wall} = 4.0$, and $\rho = 0.8$. Viscosity values obtained by using the nominal (imposed) shear rate and the actual shear rate are shown by diamonds and circles, respectively. The abscissa corresponds to nominal shear rate for diamonds and actual shear rate for circles.

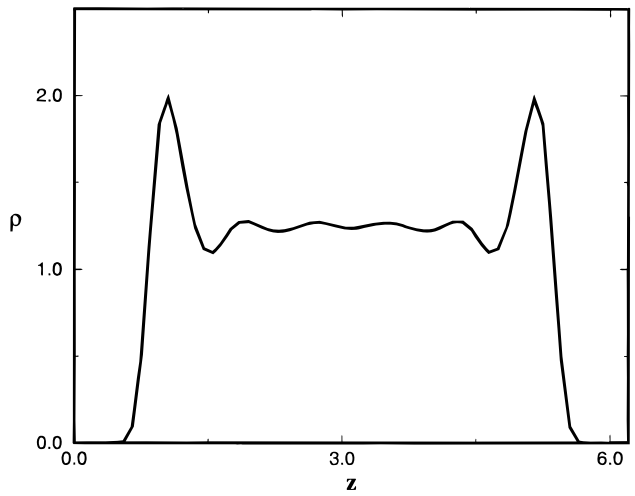

Figure 5. Site density profile for $N = 20$, $H = 6.2$, $T_{wall} = 4.0$, $\rho = 0.8$, and $\dot{\gamma} = 0.2$.

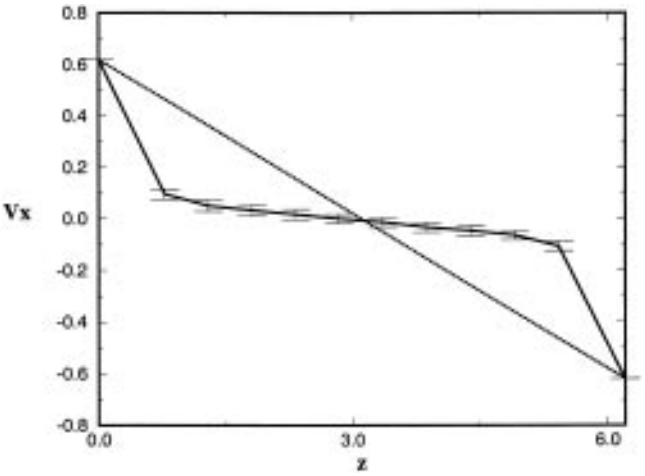

Figure 6. Velocity profile for $N = 20$, $H = 6.2$, $T_{wall} = 4.0$, $\rho = 0.8$, and $\dot{\gamma} = 0.2$. The dotted line shows the continuum prediction with no-slip boundary conditions.

identical conditions ($T = 4.0$, $\rho = 0.8$), but using homogeneous shear techniques and a Nose−Hoover thermostat to maintain a constant temperature throughout the sheared fluid. Up to a shear rate of 0.1, the viscosity values reported here are within 10% of those reported by Xu et al. The agreement is remarkable, considering that the viscosity values obtained in our work are slightly dependent on the characteristics of the wall (e.g. lattice spacing[20]). However, while shear thinning disappears beyond $\dot{\gamma} = 0.2$ in our work, Xu et al. observe shear thinning up to $\dot{\gamma} = 1.0$. We believe that such discrepancies can be attributed to the use of a thermostat in the simulations by Xu et al.[21] In the simulations reported here, the temperature rise in the fluid because of viscous heating becomes significant beyond shear rates of 0.1.

In summary, our results show that, at the shear rates typically used in molecular simulations, viscous heating can lead to a large temperature rise in the sheared fluid. This effect is even more significant for polymers than for simple fluids. The shear rate dependence of viscosity obtained from simulations depends strongly on the schemes used for controlling the temperature of the model system. In many instances, isothermal, homogeneous shear simulations are carried out to infer the zero shear viscosity of a bulk fluid by means of some extrapolation scheme. In that context, it is difficult to say whether one method is better than the other. For study of confined fluids, however, we believe that our approach of keeping the wall temperature constant closely mimics an actual experimental setup, whereas algorithms that use a thermostat to impose a constant temperature throughout the sheared fluid remove the viscous heat from the system in an unphysical manner. Our findings indicate that caution should be exercised in interpreting the results of isothermal nonequilibrium molecular dynamics simulations of fluids at high shear rates.

3.2. Effect of Confinement on Flow Properties of Confined Polymer Chains. Experimentally, it is found that the rheological properties of fluids change dramatically as the thickness of the fluid film confined between walls is decreased to molecular dimensions.[4−10] A detailed investigation of confinement effects on fluid properties was carried out by investigating the flow behavior of 20-mer chains at four different film thicknesses: 18σ, 13.6σ, 10.0σ, and 6.2σ. Other simulation conditions were kept constant at $T_{wall} = 4.0$, $\rho = 0.8$, and $\dot{\gamma} = 0.2$. Figure 5 shows the site density profile for $H = 6.2\sigma$. For the thinner film (Figure 5), the first peak of the density profile is higher than for the thicker film (Figure 1b). This is a consequence of the fact that the depletion layer near the walls constitutes a significant fraction of the total film thickness in this case, and the average density in the middle region is therefore much higher than for the thicker film. As expected, if the film is thin enough, the effect of the walls is felt over the entire film (in the form of weak oscillations in the profile) and there is no bulklike, homogeneous region.

Figure 6 depicts the velocity profile for the same conditions as in Figure 5. The effect of confinement on the velocity profile is quite dramatic. Most significantly, the slip becomes much larger when the film is made thinner. Similar behavior was observed in shear flow simulations of hexamers when the fluid film thickness was descreased from 6σ to 4σ.[19] The velocity profile is linear only in the middle region and shows some curvature for a distance of about 2σ from either wall. As a result of the large slip, the actual shear rate is much smaller than the nominal shear rate. These results suggest that the two walls essentially slide over the confined fluid, which moves with a very small velocity compared to that of the walls. It is plausible

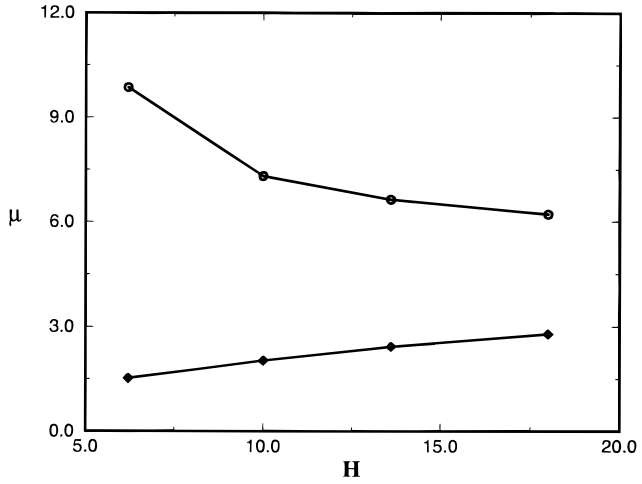

Figure 7. Viscosity of polymer ($N = 20$) as a function of film thickness. Values obtained by using nominal (imposed) shear rate and the actual shear rate are shown by diamonds and circles, respectively.

that in these narrow channels most of the chains lie on both sides of the central plane of the fluid film, thus decreasing their net motion.

As the film thickness is decreased, the temperature rise in the fluid also decreases. For example, for $H = 6.2\sigma$, the temperature rise is only 1% compared to 20% for $H = 18\sigma$. This behavior is in agreement with continuum mechanics predictions. Physically, there are two reasons for the observed behavior: the only outlet for the viscous heat generated in the system is through the walls, which are held at a constant temperature. Since the walls are closer in this case, heat removal by conduction to the walls is more efficient, thereby keeping the temperature lower. Further, due to the large slip, the actual shear rate in the fluid is small, and therefore, less heat is generated (continuum mechanics predicts that the viscous heat generated is proportional to the square of the shear rate).

It has been observed in surface forces apparatus experiments that, as the thickness of the fluid film is decreased below 6.0σ, the viscosity of the fluid increases dramatically.[4−10] Figure 7 shows the dependence of viscosity on fluid film thickness. If the viscosity is calculated by dividing the shear stress at the wall by the nominal shear rate, then a counterintuitive situation emerges in which the viscosity increases with increasing film thickness. The actual shear rate in the film, however, is significantly different from the nominal shear rate. If the viscosity is determined using the actual shear rate, then the upper curve in Figure 7 is obtained, which indicates that the actual viscosity of the fluid increases as the film thickness decreases. The latter effect is not as dramatic as that observed in experiments, but is is important to emphasize that, in our model, wall−fluid interactions are purely repulsive, i.e. the increase in viscosity is a consequence only of confinement.

3.3. Chain Conformations under Shear Flow. The most direct measure of chain dimensions is the mean square chain end-to-end distance defined via

$$\langle R_\alpha{}^2 \rangle = \langle (r_{N\alpha} - r_{1\alpha})^2 \rangle \qquad (3)$$

where $r_{j\alpha}$ is the αth ($\alpha = x$, y, or z) component of the position of bead j. The presence of the walls and the shear flow are expected to modify chain dimensions relative to a bulk fluid. Figure 8a shows the mean

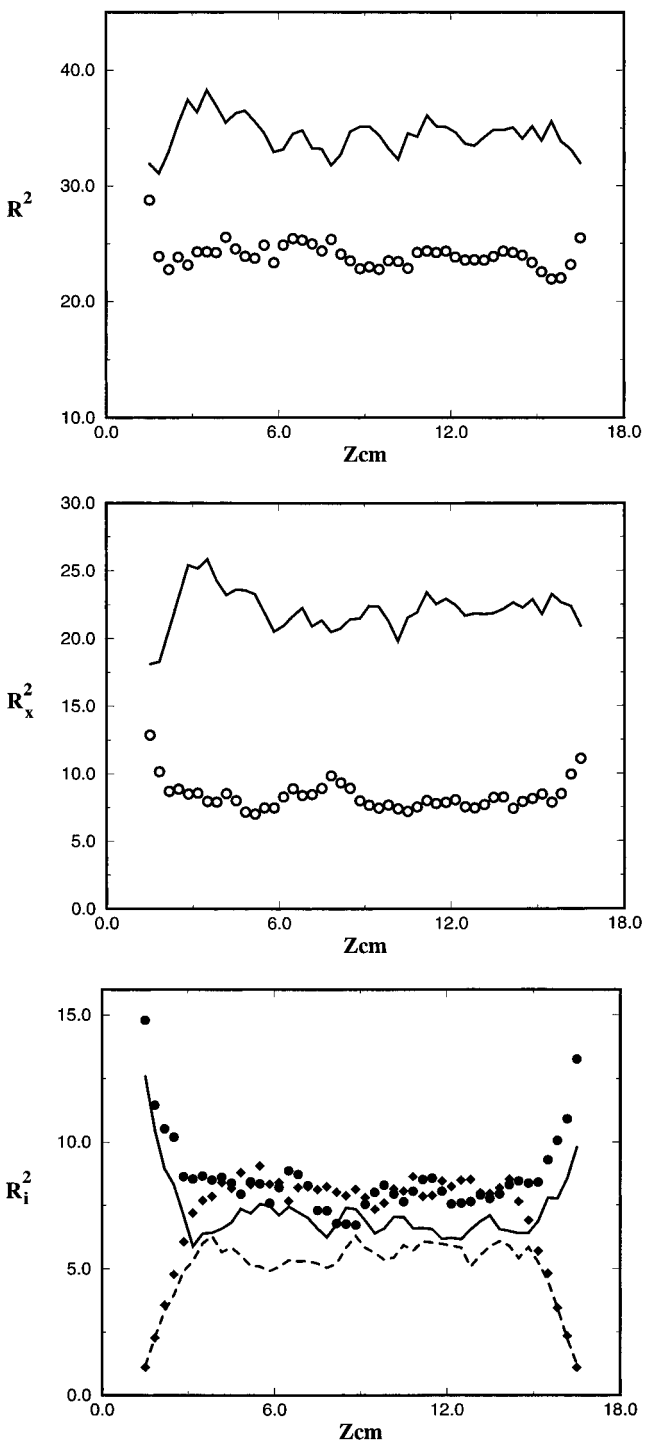

Figure 8. Mean square chain end-to-end distance and its components as a function of center of mass position: (a) $\langle R^2 \rangle$ at equilibrium (circles) and under shear (line), (b) $\langle R_x{}^2 \rangle$ at equilibrium (circles) and under shear (line), (c) $\langle R_y{}^2 \rangle$ at equilibrium (filled circles) and under shear (solid line), and $\langle R_z{}^2 \rangle$ at equilibrium (filled diamonds) and under shear (dashed line).

square end-to-end distance as a function of the distance from the center of mass to the walls, both under shear and at equilibrium. Compared to equilibrium, chains under shear have a higher mean square end-to-end dimension at all distances from the wall. Since none of the three directions—flow (x), shear gradient (z), and the vorticity or neutral direction (y)—are equivalent, it is instructive to inspect the individual components of the mean square chain end-to-end distance. Figure 8b compares the x component (flow direction) of chain dimensions under shear to that at equilibrium. Under

shear, chain dimensions are larger in the flow direction. A comparison of the *y* and *z* components under shear to those for equilibrium (Figure 8c) shows that flow effects are not as pronounced for these two directions as they are for the *x* component. Beyond a region of thickness 2σ at each wall, the three (*x*, *y*, and *z*) components of chain dimensions have the same magnitude at equilibrium. This is not the case in the sheared fluid. Very near the walls, both under shear and at equilibrium, the *y* component has a higher value while the *z* component has a lower value (compared to bulk) as expected.

It has been shown[25] that these observations regarding differences in components of chain dimensions could be a result of a flattening of chains near the walls and/or chain reorientation near the walls. A more detailed understanding of this behavior is thus obtained by investigating the shape characteristics of the chain molecules since single polymer molecules are highly anisotropic, cigar-shaped objects.[26] We investigate the shape of these molecules by representing each molecule in terms of an equivalent spheroid with the same moment of inertia. The moment of inertia tensor of molecule *i* is given by[25,27]

$$I_{i\alpha\beta} = \sum_j (r_j^2 \delta_{\alpha\beta} - r_{j\alpha} r_{j\beta}) \tag{4}$$

where $\alpha, \beta = x, y$, and *z* coordinates, $\delta_{\alpha\beta}$ is the Kronecker delta, and $r_{j\alpha}$ is the distance in the α direction of bead *j* from the center of mass. The sum is over all sites *j* of molecule *i*. Information about the shape of the molecule can then be obtained by diagonalizing the moment of inertia tensor to obtain the eigenvectors **a**, **b**, and **c** and the principal moments I_{aa}, I_{bb}, and I_{cc}. The lengths of the semiaxis vectors are given by

$$a = \left\langle \sqrt{\frac{5(I_{bb} + I_{cc} - I_{aa})}{2N}} \right\rangle \tag{5}$$

$$b = \left\langle \sqrt{\frac{5(I_{aa} + I_{cc} - I_{bb})}{2N}} \right\rangle \tag{6}$$

$$c = \left\langle \sqrt{\frac{5(I_{aa} + I_{bb} - I_{cc})}{2N}} \right\rangle \tag{7}$$

The eigenvector **a** corresponds to the smallest eigenvalue and is the molecular axis vector. Figure 9 shows a comparison of *a*, *b*, and *c* as a function of center of mass distance at equilibrium and under shear. The two semiaxes lengths *b* and *c* have approximately the same values at equilibrium and under shear. On the other hand, *a* (the longest dimension) has a larger value under shear than at equilibrium, indicating that the molecules are elongated under shear. The values of these semiaxes lengths are virtually independent of center of mass position, suggesting that the chains are not distorted appreciably as they approach the walls. The dependence of the various components of chain dimensions on the distance from the walls (as seen in Figure 8c) must therefore be due to a reorientation of the molecules near the surfaces.

The conclusion that the chains orient along the walls can be more directly reached by looking at the orientational correlation function of chain molecules as a function of distance from the walls. We define a

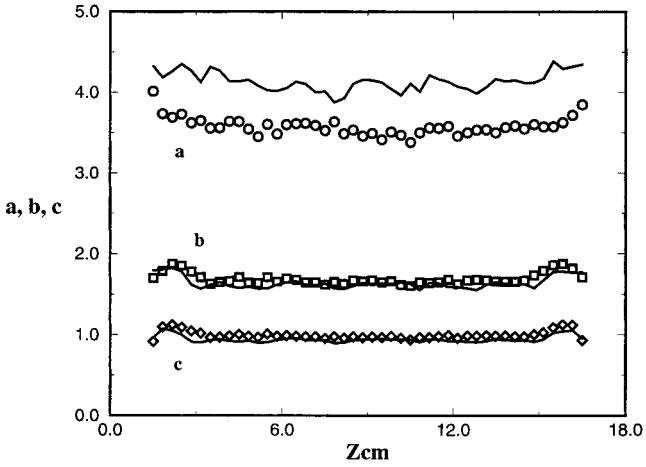

Figure 9. Semiaxis vector lengths (*a*, *b*, and *c*) of a spheroid with the same moment of inertia as the polymer molecules as a function of center of mass position at equilibrium (symbols) and under shear (lines).

molecular axis orientational correlation function, S_{2M}, by

$$S_{2M}(z) = \frac{3\langle \cos^2 \theta \rangle - 1}{2} \tag{8}$$

where *z* is the position of the chain center of mass and θ is the angle between the molecular axis vector **a** and the *z* axis. If molecules (on average) are aligned parallel to the walls, $S_{2M}(z) = -0.5$; if they are at right angles to the walls, $S_{2M}(z) = 1.0$; and if the molecules have isotropic orientations, $S_{2M}(z) = 0$. Figure 10a compares this order parameter at equilibrium and under shear. Both at equilibrium and under shear the chains are parallel to the walls for a region within 2σ from either wall. However, away from the walls, the chain orientations are isotropic at equilibrium, whereas under shear the chains still exhibit a certain degree of alignment with the flow.

The orientation of the long molecular axes parallel to the surface is accompanied by an orientation of chain segments parallel to the surface. A bond orientational correlation can be defined at the segmental level according to

$$S_{2B}(z) = \frac{3\langle \cos^2 \alpha \rangle - 1}{2} \tag{9}$$

where α is the angle between a bond (vector joining adjacent beads on a chain) and the *z* axis, and *z* is the distance of the midpoint of the bond from the walls. Figure 10b shows this bond orientational correlation function under shear and at equilibrium. In the near proximity of the wall surface (up to about 1.5σ), bonds are oriented parallel to the walls both at equilibrium and under shear. Away from the walls, bonds have an isotropic orientation at equilibrium while, under shear, the orientational correlation function has a consistent negative value at all separations, indicating that on the average individual bonds have a slight tendency to align parallel to the walls at all distances.

3.4. Slip Behavior of Polymer Chains. Contrary to conventional wisdom, recent experimental evidence suggests the occurrence of slip at polymer−wall interfaces.[1−3] For the molecular model studied here, we have carried out a systematic investigation of the effect of shear rate and molecular weight on the slip behavior

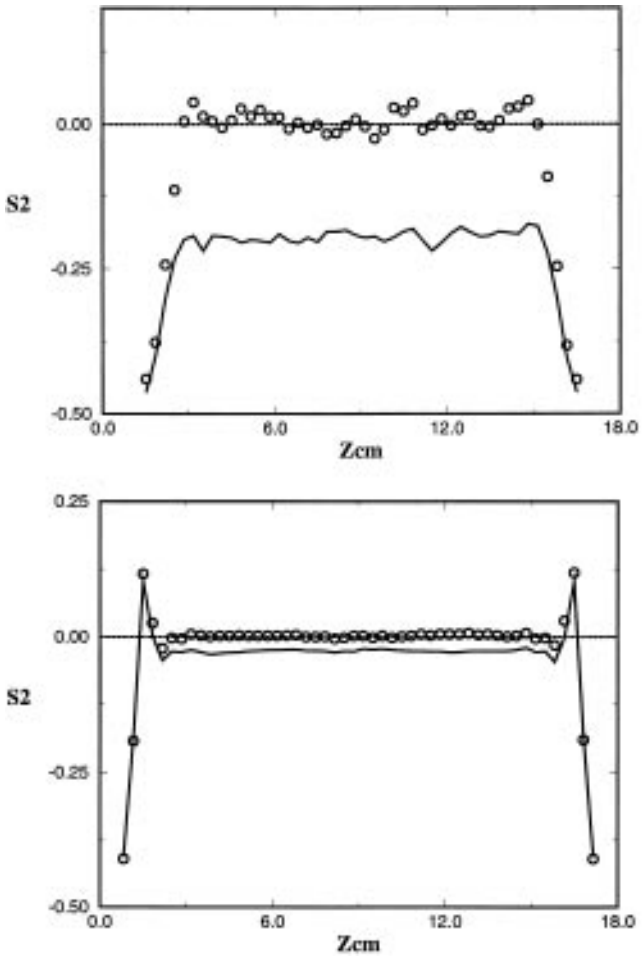

Figure 10. (a) Molecular axis orientational correlation function as a function of chain center of mass at equilibrium (circles) and under shear (line). (b) Bond orientational correlation function as a function of bond center of mass position at equilibrium (circles) and under shear (line).

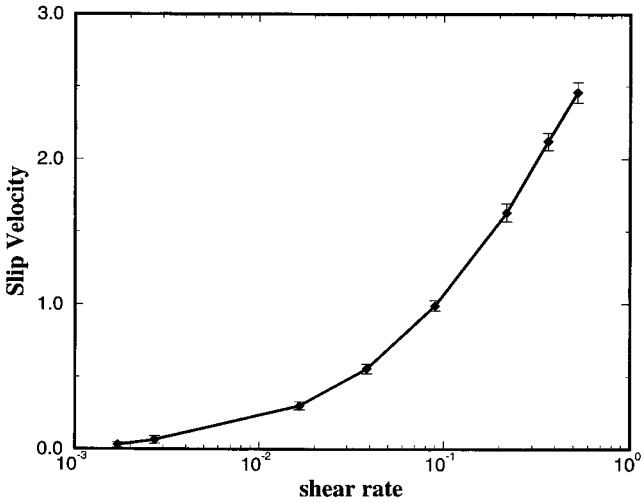

Figure 11. Slip velocity as a function of shear rate for polymeric fluid with $N = 20$. The shear rate values are the actual shear rates obtained by taking the slope of velocity profiles. Simulation conditions are $H = 18$, $\rho = 0.8$, $T_{wall} = 4.0$.

of polymer chains. The slip velocity is defined as the difference between the actual wall velocity and the velocity obtained by linearly extrapolating the velocity profile to the walls. Figure 11 shows a plot of slip velocity as a function of shear rate for chains of 20 segments. The slip velocity increases with increasing shear rate, in agreement with previous experimental results on polydimethylsiloxane melts[3] and shear flow simulations of hexamers.[19] At the lowest values of shear rate investigated the slip velocity is essentially zero. Note that these *low* shear rates ($\dot{\gamma} = 0.001$) are at least 2 orders of magnitude higher than experimental shear rates. In addition, experiments are generally carried out on much higher molecular weight polymers than considered here. Figure 12 shows the molecular weight dependence of slip velocity at a constant nominal shear rate of 0.2. As expected, up to the entanglement length ($N_e = 50$), the slip velocity monotonically increases with increasing molecular weight. Similar results were reported in previous simulations of shear flow in films of thickness 2σ, where it was shown that monomers hardly showed any slip, but chains with $N = 10-20$ showed large slip.[18] We conclude that slip has its origins in the connectivity of molecules. Beyond the entanglement length ($N_e = 50$), the slip velocity gradually decreases with further increase in molecular weight. The chain packing behavior at the walls provides a tentative explanation for this somewhat surprising finding. We find that although the site density profiles are insensitive to chain length up to N = 50, they show some dependence on chain length for N = 100 and 165, and for N = 165, the height of the first peak next to the wall is larger than that for N = 10−50. Since there is a higher number of chain sites packed next to the walls, the momentum transfer from the walls to the fluid is more efficient, thus reducing slip. We note, however that it is possible that these results could be artifacts of finite size effects at these large N values. For N = 165, the simulated system consists of 14 355 chain sites and 2500 walls atoms; it is not possible to further analyze system size dependence with our current computational resources.

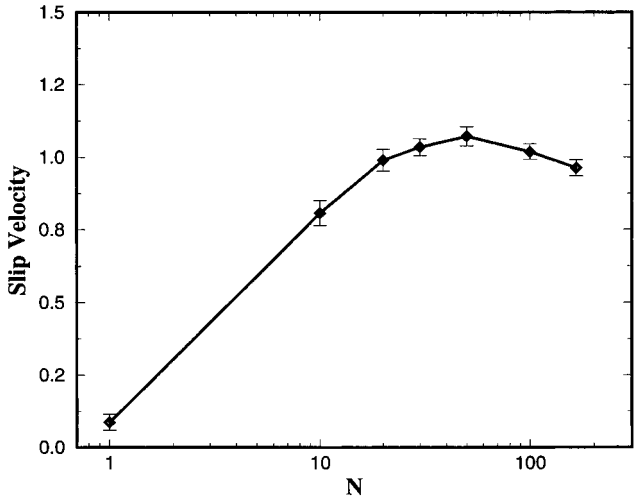

Figure 12. Slip velocity as a function of chain length (N) for nominal shear rate $\dot{\gamma} = 0.2$. Simulation conditions are $H = 18$, $\rho = 0.8$, $T_{wall} = 4.0$.

4. Conclusions

A method is presented for investigating the shear flow behavior of polymer chains confined in thin films between solid surfaces. The density profile of the polymers shows only a single layer at each wall compared to monomeric fluids, which show multiple layers at the walls. The density profiles for both monomers and polymers are insensitive to shear rate. Under shear the chains have a strong tendency to stretch and reorient in the flow direction.

At the shear rates investigated, polymer melts exhibit significant slip at the walls, the magnitude of which increases with increasing shear rate. For chain lengths smaller than the entanglement length, slip increases with chain length and reaches an approximately constant value for lengths higher than that corresponding to entanglement.

The effect of confinement on the rheological properties of polymer chains was also studied by varying the fluid film thickness. The results indicate that the apparent viscosity of the fluid decreases with a decrease in film thickness. This observation, however, is an artifact of velocity slip at the walls, the magnitude of which also increases with decreasing film thickness. If one accounts for the slip by using the actual shear rate (slope of velocity profile), the viscosity is seen to increase with decreasing film thickness, in agreement with surface forces apparatus experiments.[4−10]

It is important to note that we observe slip at the walls in simulations for which all interactions—fluid−fluid and wall−fluid—are identical. This certainly is not the case in practice, and slip behavior will definitely be a strong function of the relative magnitudes of these interactions.[1] We are currently investigating these effects for more realistic, atomistically detailed models of polymeric chains and walls. The effects of chain architecture on rheological properties of the polymeric fluids are also under investigation.

Acknowledgment. The authors thank Professors Bird and Curtiss for many insightful discussions. This work was supported by the National Science Foundation (grant numbers CTS 9409856 and CHE 9502320 to A.Y., grant number CTS 9358406 to J.J.d.P., and equipment grant number CHE 9007850 to the Chemistry Department). Acknowledgment is made to the donors of the Petroleum Research Fund, administered by the American Chemical Society, for partial support of this research.

References and Notes

(1) Ramamurthy, A. V. *J. Rheol.* **1986**, *30*, 337.
(2) Kalika, D. S.; Denn, M. M. *J. Rheol.* **1987**, *31*, 815.
(3) Migler, K. B.; Hervet, H.; Leger, L. *Phys. Rev. Lett.* **1993**, *70*, 287.
(4) Chan, D. Y. C.; Horn, R. G. *J. Chem. Phys.* **1985**, *83*, 5311.
(5) Israelachvili, J. N.; McGuiggan, P. M.; Homola, A. M. *Science* **1988**, *240*, 189.
(6) Gee, M. L.; McGuiggan, P. M.; Israelachvili, J. N.; Homola, A. M. *J. Chem. Phys.* **1990**, *93*, 1895.
(7) Van Alsten, J.; Granick, S. *Phys. Rev. Lett.* **1988**, *61*, 2570.
(8) Van Alsten, J.; Granick, S. *Macromolecules* **1990**, *23*, 4856.
(9) Hu, H.-W.; Carson, G. A.; Granick, S. *Phys. Rev. Lett.* **1991**, *66*, 2758.
(10) Granick, S. *Science* **1991**, *253*, 1374.
(11) Evans, D. J.; Morriss, G. P. *Statistical Mechanics of Nonequilibrium Liquids*; Academic: London, U.K., 1990.
(12) Ashurst, W. T.; Hooever, W. G. *Phys. Rev. A* **1975**, *11*, 658.
(13) Trozzi, C.; Ciccotti, G. *Phys. Rev. A* **1984**, *29*, 916.
(14) Bitsanis, I.; Magda, J. J.; Tirrell, M.; Davis, H. T. *J. Chem. Phys.* **1987**, *87*, 1733.
(15) Bitsanis, I.; Somers, S. A.; Davis, H. T.; Tirrell, M. *J. Chem. Phys.* **1990**, *93*, 3427.
(16) Thompson, P. A.; Robbins, M. O. *Phys. Rev. A* **1990**, *41*, 6830.
(17) Thompson, P. A.; Grest, G. S.; Robbins, M. O. *Phys. Rev. Lett.* **1992**, *68*, 3448.
(18) Thompson, P. A.; Robbins, M. O.; Grest, G. S. *Isr. J. of Chem.* **1995**, *35*, 93.
(19) Manias, E.; Hadziioannou, G.; Bitsanis, I.; Ten Brinke, G. *Europhys. Lett.* **1993**, *24*, 99.
(20) Khare, R.; de Pablo, J. J.; Yethiraj, A., submitted to *J. Chem. Phys.*
(21) Xu, Z.; de Pablo, J. J.; Kim, S. *J. Chem. Phys.* **1995**, *102*, 5836.
(22) Allen, M. P.; Tildesley, D. J. *Computer Simulation of Liquids*; Oxford University: Oxford, U.K., 1992.
(23) Yethiraj, A.; Hall, C. K. *Macromolecules* **1990**, *23*, 1635.
(24) Bitsanis, I.; Hadziioannou, G. *J. Chem. Phys.* **1990**, *92*, 3827.
(25) Yethiraj, A. *J. Chem. Phys.* **1994**, *101*, 2489.
(26) Solc, K.; Stockmayer, W. H. *J. Chem. Phys.* **1971**, *54*, 2756.
(27) Wilson, M. R.; Allen, M. P. *Mol. Phys.* **1993**, *80*, 277.

MA960083X